Measurement of the Inclusive Electron Neutrino Charged Current Cross Section on Carbon with the T2K Near Detector

K. Abe,[46] J. Adam,[32] H. Aihara,[45,23] T. Akiri,[9] C. Andreopoulos,[44] S. Aoki,[24] A. Ariga,[2] S. Assylbekov,[8] D. Autiero,[29] M. Barbi,[39] G. J. Barker,[54] G. Barr,[35] M. Bass,[8] M. Batkiewicz,[13] F. Bay,[11] V. Berardi,[18] B. E. Berger,[8,23] S. Berkman,[4] S. Bhadra,[58] F. d. M. Blaszczyk,[28] A. Blondel,[12] C. Bojechko,[51] S. Bordoni,[15] S. B. Boyd,[54] D. Brailsford,[17] A. Bravar,[12] C. Bronner,[23] N. Buchanan,[8] R. G. Calland,[27] J. Caravaca Rodríguez,[15] S. L. Cartwright,[42] R. Castillo,[15] M. G. Catanesi,[18] A. Cervera,[16] D. Cherdack,[8] G. Christodoulou,[27] A. Clifton,[8] J. Coleman,[27] S. J. Coleman,[7] G. Collazuol,[20] K. Connolly,[55] L. Cremonesi,[38] A. Dabrowska,[13] I. Danko,[37] R. Das,[8] S. Davis,[55] P. de Perio,[49] G. De Rosa,[19] T. Dealtry,[44,35] S. R. Dennis,[54,44] C. Densham,[44] D. Dewhurst,[35] F. Di Lodovico,[38] S. Di Luise,[11] O. Drapier,[10] T. Duboyski,[38] K. Duffy,[35] J. Dumarchez,[36] S. Dytman,[37] M. Dziewiecki,[53] S. Emery-Schrenk,[6] A. Ereditato,[2] L. Escudero,[16] A. J. Finch,[26] M. Friend,[14,†] Y. Fujii,[14,†] Y. Fukuda,[30] A. P. Furmanski,[54] V. Galymov,[29] S. Giffin,[39] C. Giganti,[36] K. Gilje,[32] D. Goeldi,[2] T. Golan,[57] M. Gonin,[10] N. Grant,[26] D. Gudin,[22] D. R. Hadley,[54] A. Haesler,[12] M. D. Haigh,[54] P. Hamilton,[17] D. Hansen,[37] T. Hara,[24] M. Hartz,[23,50] T. Hasegawa,[14,†] N. C. Hastings,[39] Y. Hayato,[46,23] C. Hearty,[4,‡] R. L. Helmer,[50] M. Hierholzer,[2] J. Hignight,[32] A. Hillairet,[51] A. Himmel,[9] T. Hiraki,[25] S. Hirota,[25] J. Holeczek,[43] S. Horikawa,[11] K. Huang,[25] A. K. Ichikawa,[25] K. Ieki,[25] M. Ieva,[15] M. Ikeda,[46] J. Imber,[32] J. Insler,[28] T. J. Irvine,[47] T. Ishida,[14,†] T. Ishii,[14,†] E. Iwai,[14] K. Iwamoto,[40] K. Iyogi,[46] A. Izmaylov,[16,22] A. Jacob,[35] B. Jamieson,[56] R. A. Johnson,[7] J. H. Jo,[32] P. Jonsson,[17] C. K. Jung,[32,§] M. Kabirnezhad,[31] A. C. Kaboth,[17] T. Kajita,[47,§] H. Kakuno,[48] J. Kameda,[46] Y. Kanazawa,[45] D. Karlen,[51,50] I. Karpikov,[22] T. Katori,[38] E. Kearns,[3,23,§] M. Khabibullin,[22] A. Khotjantsev,[22] D. Kielczewska,[52] T. Kikawa,[25] A. Kilinski,[31] J. Kim,[4] J. Kisiel,[43] P. Kitching,[1] T. Kobayashi,[14,†] L. Koch,[41] A. Kolaceke,[39] A. Konaka,[50] L. L. Kormos,[26] A. Korzenev,[12] Y. Koshio,[33,§] W. Kropp,[5] H. Kubo,[25] Y. Kudenko,[22,‖] R. Kurjata,[53] T. Kutter,[28] J. Lagoda,[31] I. Lamont,[26] E. Larkin,[54] M. Laveder,[20] M. Lawe,[42] M. Lazos,[27] T. Lindner,[50] C. Lister,[54] R. P. Litchfield,[54] A. Longhin,[20] L. Ludovici,[21] L. Magaletti,[18] K. Mahn,[50] M. Malek,[17] S. Manly,[40] A. D. Marino,[7] J. Marteau,[29] J. F. Martin,[49] S. Martynenko,[22] T. Maruyama,[14,†] V. Matveev,[22] K. Mavrokoridis,[27] E. Mazzucato,[6] M. McCarthy,[4] N. McCauley,[27] K. S. McFarland,[40] C. McGrew,[32] C. Metelko,[27] P. Mijakowski,[31] C. A. Miller,[50] A. Minamino,[25] O. Mineev,[22] A. Missert,[7] M. Miura,[46,§] S. Moriyama,[46,§] Th. A. Mueller,[10] A. Murakami,[25] M. Murdoch,[27] S. Murphy,[11] J. Myslik,[51] T. Nakadaira,[14,†] M. Nakahata,[46,23] K. Nakamura,[23,14,†] S. Nakayama,[46,§] T. Nakaya,[25,23] K. Nakayoshi,[14,†] C. Nielsen,[4] M. Nirkko,[2] K. Nishikawa,[14,†] Y. Nishimura,[47] H. M. O'Keeffe,[26] R. Ohta,[14,†] K. Okumura,[47,23] T. Okusawa,[34] W. Oryszczak,[52] S. M. Oser,[4] R. A. Owen,[38] Y. Oyama,[14,†] V. Palladino,[19] J. L. Palomino,[32] V. Paolone,[37] D. Payne,[27] O. Perevozchikov,[28] J. D. Perkin,[42] Y. Petrov,[4] L. Pickard,[42] E. S. Pinzon Guerra,[58] C. Pistillo,[2] P. Plonski,[53] E. Poplawska,[38] B. Popov,[36,¶] M. Posiadala,[52] J.-M. Poutissou,[50] R. Poutissou,[50] P. Przewlocki,[31] B. Quilain,[10] E. Radicioni,[18] P. N. Ratoff,[26] M. Ravonel,[12] M. A. M. Rayner,[12] A. Redij,[2] M. Reeves,[26] E. Reinherz-Aronis,[8] P. A. Rodrigues,[40] P. Rojas,[8] E. Rondio,[31] S. Roth,[41] A. Rubbia,[11] D. Ruterbories,[40] R. Sacco,[38] K. Sakashita,[14,†] F. Sánchez,[15] F. Sato,[14] E. Scantamburlo,[12] K. Scholberg,[9,†] S. Schoppmann,[41] J. Schwehr,[8] M. Scott,[50] Y. Seiya,[34] T. Sekiguchi,[14,†] H. Sekiya,[46,§] D. Sgalaberna,[11] M. Shiozawa,[46,23] S. Short,[38] Y. Shustrov,[22] P. Sinclair,[17] B. Smith,[17] M. Smy,[5] J. T. Sobczyk,[57] H. Sobel,[5,23] M. Sorel,[16] L. Southwell,[26] P. Stamoulis,[16] J. Steinmann,[41] B. Still,[38] Y. Suda,[45] A. Suzuki,[24] K. Suzuki,[25] S. Y. Suzuki,[14,†] Y. Suzuki,[23,23] R. Tacik,[39,50] M. Tada,[14,†] S. Takahashi,[25] A. Takeda,[46] Y. Takeuchi,[24,23] H. K. Tanaka,[46,§] H. A. Tanaka,[4,‡] M. M. Tanaka,[14,†] D. Terhorst,[41] R. Terri,[38] L. F. Thompson,[42] A. Thorley,[27] S. Tobayama,[4] W. Toki,[8] T. Tomura,[46] Y. Totsuka,[*] C. Touramanis,[27] T. Tsukamoto,[14,†] M. Tzanov,[28] Y. Uchida,[17] A. Vacheret,[35] A. Vagins,[23,5] G. Vasseur,[6] T. Wachala,[13] A. V. Waldron,[35] C. W. Walter,[9,§] D. Wark,[44,17] M. O. Wascko,[17] A. Weber,[44,35] R. Wendell,[46,§] R. J. Wilkes,[55] M. J. Wilking,[50] C. Wilkinson,[42] Z. Williamson,[35] J. R. Wilson,[38] R. J. Wilson,[8] T. Wongjirad,[9] Y. Yamada,[14,†] K. Yamamoto,[34] C. Yanagisawa,[32,**] T. Yano,[24] S. Yen,[50] N. Yershov,[22] M. Yokoyama,[45,†] T. Yuan,[7] M. Yu,[58] A. Zalewska,[13] J. Zalipska,[31] L. Zambelli,[14,†] K. Zaremba,[53] M. Ziembicki,[53] E. D. Zimmerman,[7] M. Zito,[6] and J. Żmuda[57]

(T2K Collaboration)

[1]Department of Physics, University of Alberta, Centre for Particle Physics, Edmonton, Alberta, Canada
[2]Albert Einstein Center for Fundamental Physics, Laboratory for High Energy Physics (LHEP), University of Bern, Bern, Switzerland
[3]Department of Physics, Boston University, Boston, Massachusetts, USA
[4]Department of Physics and Astronomy, University of British Columbia, Vancouver, British Columbia, Canada
[5]Department of Physics and Astronomy, University of California, Irvine, Irvine, California, USA

[6]IRFU, CEA Saclay, Gif-sur-Yvette, France

[7]Department of Physics, University of Colorado at Boulder, Boulder, Colorado, USA

[8]Department of Physics, Colorado State University, Fort Collins, Colorado, USA

[9]Department of Physics, Duke University, Durham, North Carolina, USA

[10]Laboratoire Leprince-Ringuet, Ecole Polytechnique, IN2P3-CNRS, Palaiseau, France

[11]Institute for Particle Physics, ETH Zurich, Zurich, Switzerland

[12]Section de Physique, University of Geneva, DPNC, Geneva, Switzerland

[13]H. Niewodniczanski Institute of Nuclear Physics PAN, Cracow, Poland

[14]High Energy Accelerator Research Organization (KEK), Tsukuba, Ibaraki, Japan

[15]Institut de Fisica d'Altes Energies (IFAE), Bellaterra (Barcelona), Spain

[16]IFIC (CSIC & University of Valencia), Valencia, Spain

[17]Department of Physics, Imperial College London, London, United Kingdom

[18]Dipartimento Interuniversitario di Fisica, INFN Sezione di Bari and Università e Politecnico di Bari, Bari, Italy

[19]Dipartimento di Fisica, INFN Sezione di Napoli and Università di Napoli, Napoli, Italy

[20]Dipartimento di Fisica, INFN Sezione di Padova and Università di Padova, Padova, Italy

[21]INFN Sezione di Roma and Università di Roma "La Sapienza", Roma, Italy

[22]Institute for Nuclear Research of the Russian Academy of Sciences, Moscow, Russia

[23]Kavli Institute for the Physics and Mathematics of the Universe (WPI), Todai Institutes for Advanced Study,
University of Tokyo, Kashiwa, Chiba, Japan

[24]Kobe University, Kobe, Japan

[25]Department of Physics, Kyoto University, Kyoto, Japan

[26]Physics Department, Lancaster University, Lancaster, United Kingdom

[27]Department of Physics, University of Liverpool, Liverpool, United Kingdom

[28]Department of Physics and Astronomy, Louisiana State University, Baton Rouge, Louisiana, USA

[29]Université de Lyon, Université Claude Bernard Lyon 1, IPN Lyon (IN2P3), Villeurbanne, France

[30]Department of Physics, Miyagi University of Education, Sendai, Japan

[31]National Centre for Nuclear Research, Warsaw, Poland

[32]Department of Physics and Astronomy, State University of New York at Stony Brook, Stony Brook, New York, USA

[33]Department of Physics, Okayama University, Okayama, Japan

[34]Department of Physics, Osaka City University, Osaka, Japan

[35]Department of Physics, Oxford University, Oxford, United Kingdom

[36]Laboratoire de Physique Nucléaire et de Hautes Energies (LPNHE), UPMC,
Université Paris Diderot, CNRS/IN2P3, Paris, France

[37]Department of Physics and Astronomy, University of Pittsburgh, Pittsburgh, Pennsylvania, USA

[38]School of Physics and Astronomy, Queen Mary University of London, London, United Kingdom

[39]Department of Physics, University of Regina, Regina, Saskatchewan, Canada

[40]Department of Physics and Astronomy, University of Rochester, Rochester, New York, USA

[41]RWTH Aachen University, III. Physikalisches Institut, Aachen, Germany

[42]Department of Physics and Astronomy, University of Sheffield, Sheffield, United Kingdom

[43]Institute of Physics, University of Silesia, Katowice, Poland

[44]STFC, Rutherford Appleton Laboratory, Harwell Oxford, and Daresbury Laboratory, Warrington, United Kingdom

[45]Department of Physics, University of Tokyo, Tokyo, Japan

[46]Institute for Cosmic Ray Research, University of Tokyo, Kamioka Observatory, Kamioka, Japan

[47]Institute for Cosmic Ray Research, University of Tokyo, Research Center for Cosmic Neutrinos, Kashiwa, Japan

[48]Department of Physics, Tokyo Metropolitan University, Tokyo, Japan

[49]Department of Physics, University of Toronto, Toronto, Ontario, Canada

[50]TRIUMF, Vancouver, British Columbia, Canada

[51]Department of Physics and Astronomy, University of Victoria, Victoria, British Columbia, Canada

[52]Faculty of Physics, University of Warsaw, Warsaw, Poland

[53]Institute of Radioelectronics, Warsaw University of Technology, Warsaw, Poland

[54]Department of Physics, University of Warwick, Coventry, United Kingdom

[55]Department of Physics, University of Washington, Seattle, Washington, USA

[56]Department of Physics, University of Winnipeg, Winnipeg, Manitoba, Canada

[57]Faculty of Physics and Astronomy, Wroclaw University, Wroclaw, Poland

[58]Department of Physics and Astronomy, York University, Toronto, Ontario, Canada

The T2K off-axis near detector ND280 is used to make the first differential cross-section measurements of electron neutrino charged current interactions at energies ~1 GeV as a function of electron momentum, electron scattering angle, and four-momentum transfer of the interaction. The total flux-averaged ν_e charged

current cross section on carbon is measured to be $\langle\sigma\rangle_\phi = 1.11 \pm 0.10(\text{stat}) \pm 0.18(\text{syst}) \times 10^{-38}$ cm^2/nucleon. The differential and total cross-section measurements agree with the predictions of two leading neutrino interaction generators, NEUT and GENIE. The NEUT prediction is 1.23×10^{-38} cm^2/nucleon and the GENIE prediction is 1.08×10^{-38} cm^2/nucleon. The total ν_e charged current cross-section result is also in agreement with data from the Gargamelle experiment.

Introduction.—T2K is a long baseline neutrino oscillation experiment measuring ν_e appearance and ν_μ disappearance from a ν_μ beam. Neutrino oscillations are described by a mixing matrix parametrized by three mixing angles and a *CP* violating phase, δ_{CP} [1,2]. The three mixing angles have been measured to better than 10% precision [3], and measuring δ_{CP} is currently a major goal in neutrino physics [4].

Future ν_e appearance measurements can be used to search for *CP* violation in neutrino interactions, and these rely on precise understanding of both ν_μ and ν_e charged-current (CC) interaction cross sections at energies ~ 1 GeV. Many ν_μ cross-section measurements have been made at the GeV scale, both of the total CC inclusive cross section and of individual interaction modes (see Ref. [5] for a review of cross-section data, and Refs. [6–8] for recent results). Only the Gargamelle experiment has measured the ν_e CC inclusive cross section at the GeV scale [9], and there are currently no ν_e differential cross-section results as a function of the electron kinematics. Theoretical differences are expected between the ν_e and ν_μ cross sections [10], and measuring these with data is critical to understand the systematic uncertainties related to the search for *CP* violation in the lepton sector. The uncertainty in ν_e cross sections will become increasingly important in future oscillation experiments as statistical and other systematic uncertainties are reduced.

In this Letter we present the first ν_e CC inclusive differential cross-section measurements for neutrinos with energy ~ 1 GeV as a function of the electron momentum (p_e), electron scattering angle [$\cos(\theta_e)$], and the four-momentum transfer of the interaction (Q^2_{QE}). The total flux-averaged CC inclusive cross section is also presented.

T2K experiment.—T2K [11] operates from the J-PARC facility in Tokai, Japan. A muon neutrino beam is produced from the decay of charged pions and kaons generated by 30 GeV proton collisions on a graphite target and focused by three magnetic horns. Downstream of the horns is the decay volume, 96 m in length, followed by the beam dump and muon monitors (MUMON [12]). The neutrino beam illuminates an on-axis near detector (INGRID [13]), an off-axis near detector (ND280), and an off-axis far detector (Super-Kamiokande [14]). The off-axis detectors are positioned at an angle of 2.5° relative to the beam axis direction. The near detectors are located 280 m from the target and are used to determine the neutrino beam direction, spectrum, and composition before oscillations, and to measure neutrino cross sections. Super-Kamiokande, a 50 kt water

Cherenkov detector situated 295 km away, is used to detect the neutrinos after oscillation.

ND280 is a magnetized multipurpose detector designed to measure interactions of both ν_μ and ν_e from the T2K beam before oscillations. It is composed of a number of subdetectors installed inside the refurbished UA1/NOMAD magnet, which provides a magnetic field of 0.2 T. The central subdetectors form a tracking detector, composed of two fine-grained scintillator detectors (FGDs [15]) and three time projection chambers (TPCs [16]). The FGDs are used as the target for the neutrino interactions, and while the upstream FGD (FGD1) is composed solely of scintillator bars, the downstream FGD (FGD2) also contains water layers. Upstream of the tracker is a π^0 detector (P0D [17]), explicitly built to measure neutrino interactions with a π^0 in the final state. The tracker and P0D are surrounded by a set of electromagnetic calorimeters (ECals [18]), and the magnet yokes are instrumented with side muon range detectors (SMRDs [19]) to track high angle muons.

The results presented here are based on data taken from January 2010 to May 2013. During this period the proton beam power has steadily increased and reached 220 kW continuous operation with a world record of 1.2×10^{14} protons per pulse. The physics-quality data for this analysis correspond to a total of 5.90×10^{20} protons on target (p.o.t.).

Neutrino beam flux.—The neutrino beam flux [20] is predicted by modeling interactions of the primary beam protons with a graphite target using the FLUKA2008 package [21] and external hadron production data from the CERN NA61/SHINE experiment [22,23]. GEANT3 [24] with GCALOR [25] is used to simulate the propagation of secondary and tertiary pions and kaons, and their decays into neutrinos. Decays of kaons and muons, in the decay volume, create the approximately 1% ν_e component of the beam. Muon decays are the dominant source of ν_e with energies below 1 GeV, with higher energy neutrinos produced by kaon decays.

The neutrino flux uncertainties are dominated by hadron production uncertainties, with contributions from the neutrino beam direction and the proton beam uncertainties. The neutrino beam direction—monitored indirectly by MUMON on a spill-by-spill basis, and directly by INGRID [26]—has been well within the required ± 1 mrad during the full run period. The neutrino interaction rate per p.o.t. has also been measured by INGRID, and is stable within 0.7%. The total systematic uncertainty on the ν_e flux is 13% at the mean ν_e energy (1.3 GeV).

Selection of electron neutrino interactions in ND280.—
Full details of the event selections can be found in
Ref. [27], where the only difference is that in this analysis
only interactions in FGD1 are selected, rather than FGD1
and FGD2. This is so that interactions on water in FGD2
are not included.

Electron neutrino interactions are selected using the
highest momentum negative track starting inside the fiducial
volume of FGD1. To reduce the large background from ν_μ
charged-current interactions, electron particle identification
criteria are applied using TPC dE/dx and ECal shape and
energy measurements. These remove 99.9% of μ^- tracks,
and although a clean sample of e^- is selected, 62.4% of
events are from photons which produce e^+e^- pairs in FGD1.
This γ background is reduced by searching for a positron and
applying an invariant mass cut, and vetoing on activity in
TPC1, the P0D, and ECals upstream of FGD1. After this
procedure, 315 ν_e CC interaction candidates are selected,
with an expected purity of 65%. The reconstructed momen-
tum, scattering angle, and Q^2_{QE} distributions are shown in
Fig. 1, and compared to the prediction from the NEUT
neutrino interaction generator [28]. Q^2_{QE} is the reconstructed
Q^2 assuming CC quasielastic (CCQE) kinematics [29], with
a stationary target nucleon and 25 MeV binding energy.

The background from $\gamma \to e^+e^-$ conversions in the ν_e
sample is 23%, 70% of which are from neutrinos inter-
actions outside the FGD1 fiducial volume. A control
sample, referred to as the γ sample, is used to constrain
this, and is selected by finding electron-positron pairs that
enter the TPC and that have a low invariant mass. The data
show a deficit at low momentum in both the ν_e and γ
samples. This deficit is also visible in Ref. [27], which
selects events in FGD2 as well as FGD1.

Unfolding method.—The Bayesian technique by
d'Agostini [30] is used to unfold from the measured
reconstructed distributions to the underlying true distribu-
tions. For each observable, the true (reconstructed) bins are
denoted by t_k (r_j). There are n_t (n_r) true (reconstructed)
bins in total. Bayes' theorem is used to generate the
unsmearing matrix

$$P(t_k|r_j) = \frac{P(r_j|t_k)P(t_k)}{\sum_{\alpha=1}^{n_t} P(r_j|t_\alpha)P(t_\alpha)}, \quad (1)$$

where $P(r_j|t_k)$ is the smearing matrix and $P(t_k)$ is the
Monte Carlo (MC) prior probability of finding a signal
event in true bin t_k. Given a data set $N_{r_j}^{\text{meas}}$, the estimated
number of events in each true bin is given by

$$N_{t_k} = \frac{1}{\epsilon_{t_k}} \sum_{j=1}^{n_r} P(t_k|r_j)(N_{r_j}^{\text{meas}} - B_{r_j}), \quad (2)$$

where B_{r_j} is the number of background events that were
selected and ϵ_{t_k} is the efficiency of detecting a signal event
in bin t_k. The unfolding is performed separately for each
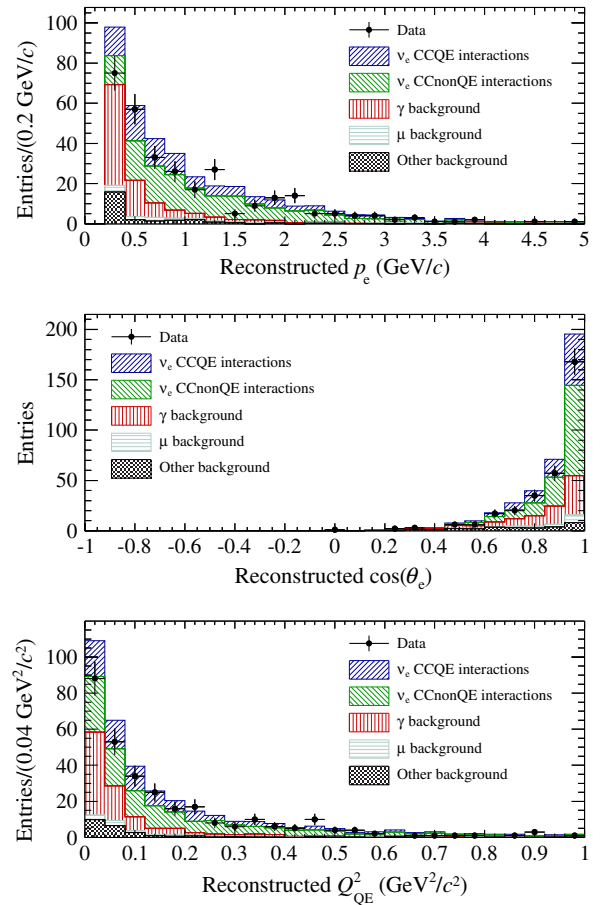variable. For defining the true bin of each interaction, the

FIG. 1 (color online). Reconstructed p_e (top), $\cos(\theta_e)$ (middle),
and Q^2_{QE} (bottom) distributions of ν_e event candidates. The
NEUT MC prediction is separated into the ν_e CC interaction
signals from CCQE and CCnonQE interactions, background
from $\gamma \to e^+e^-$ conversions, background from μ^- tracks and all
other backgrounds.

true final state momentum and angle of the electron and the
CCQE effective Q^2 of the interaction (calculated using
the true final state electron kinematics), Q^2_{QE}, are used. The
NEUT neutrino generator is used for the unfolding results
presented in this Letter.

The Bayesian unfolding technique was also used in
Ref. [6] for measuring the ν_μ CC inclusive cross section
with ND280. The main difference in the unfolding method
for this analysis is that the MC background prediction B_{r_j} is
estimated using the γ sample. Specifically, the background
from neutrino interactions occurring outside of the fiducial
volume (out-of-fiducial events) is reweighted based on the
γ sample data. This choice is made as the systematic
uncertainties relating to in-fiducial events have been well
studied, 30% of the out-of-fiducial events are on heavy
targets (iron and lead) and 66% are from interaction
channels on which there are large uncertainties in the
modeling (deep inelastic scattering and neutral current
interactions). The MC prediction of events in the fiducial
volume is subtracted from the γ sample data, and the

data-MC ratio of the out-of-fiducial events is then computed in $[p_e, \cos(\theta_e)]$ bins. The out-of-fiducial component of the ν_e sample is reweighted based on this data-MC ratio distribution. The two-dimensional reweighting scheme is chosen as the ν_e and γ samples preferentially select photons from different origins: the γ sample requires both the e^+ and e^- to be reconstructed, so preferentially selects higher-energy and more forwards-going photons.

The effect of systematic uncertainties on the cross-section measurements are computed using the same covariance matrix method as in Ref. [6]. Separate covariance matrices are computed for the data statistics, the MC statistics, detector systematics, flux and cross-section systematics, and out-of-fiducial systematics. One thousand toy experiments are performed to generate each matrix, and each experiment simultaneously affects both the ν_e and γ samples.

The data statistical uncertainty is evaluated by varying the contents of each data bin according to Poisson statistics. The MC statistical uncertainty is evaluated by separately varying the ν_e, the in-fiducial background, and the out-of-fiducial background components according to Poisson statistics. Detector systematics are studied by varying parameters such as the momentum resolution, and propagating the effect to the selection. The TPC, FGD, ECal, and external interaction uncertainties are described in detail in Ref. [27]. The uncertainty on the FGD mass is 0.67% [6]. The flux and cross-section uncertainties are also described in Ref. [27]. The flux uncertainties are based on beam line measurements and hadron production data. The cross-section uncertainties, including neutrino-nucleon, nuclear modeling, pion production, and final state interaction uncertainties are constrained using external data and comparisons between different nuclear models [29]; these uncertainties affect signal efficiencies and background spectra.

Due to the discrepancy between data and simulation for the γ sample, conservatively an extra systematic is applied to the out-of-fiducial volume reweighting in addition to the statistical uncertainty of the γ sample. If the reweighting factor in a given bin is α, then the correction is modeled as a Gaussian with mean α and width $\alpha/3$. Values of α range between 0.1 and 0.75 for bins with a total γ background of more than 5%.

Cross-section results.—The signal for this analysis is all ν_e CC interactions occurring in the FGD1 fiducial volume. FGD1 is composed of carbon (86.1% by mass), hydrogen (7.4%), oxygen (3.7%), titanium (1.7%), silicon (1.0%), and nitrogen (0.1%). The analysis measures the flux-averaged differential ν_e CC inclusive cross section, and for bin t_k of variable X, this is given by

$$\left\langle \frac{\partial \langle \sigma \rangle_\phi}{\partial X} \right\rangle_{t_k} = \frac{N_{t_k}}{\Delta X_{t_k} T \phi}, \qquad (3)$$

where X is either p_e, $\cos(\theta_e)$ or Q^2, ΔX_{t_k} is the width of the bin, N_{t_k} is the total number of signal events in the bin, T is

the number of target nucleons (5.5×10^{29} [6]), ϕ is the total integrated flux (1.35×10^{11} cm^{-2}), and $\langle \cdots \rangle_\phi$ indicates that the quantity is averaged over the flux.

The total flux averaged cross section per nucleon is computed by summing over all X bins, as

$$\langle \sigma \rangle_\phi = \frac{\sum_{k=1}^{n_t} N_{t_k}}{T \phi}. \qquad (4)$$

For comparison, differential and total flux-averaged cross-section predictions are computed using the NEUT (version 5.1.4.2) and GENIE (version 2.6.4 [31]) generators.

Figure 2 shows the unfolded differential cross-section results as a function of p_e, $\cos(\theta_e)$, and Q^2_{QE}. The data
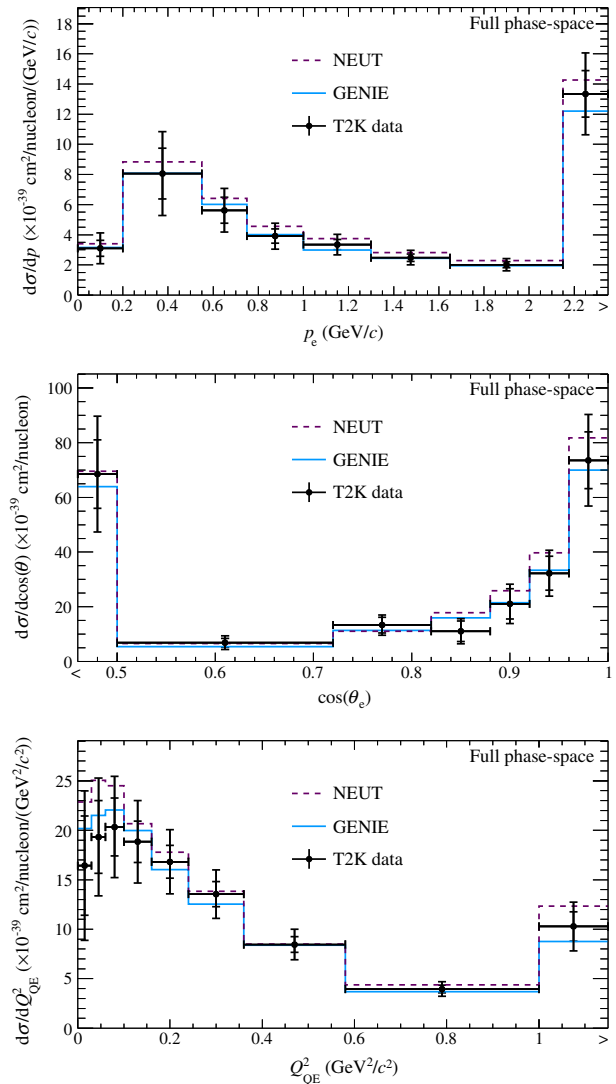

FIG. 2 (color online).   Unfolded ν_e CC inclusive differential cross sections as a function of p_e (top), $\cos(\theta_e)$ (middle), and Q^2_{QE} (bottom). The inner (outer) error bars show the statistical (total) uncertainty on the data. The dashed (solid) line shows the NEUT (GENIE) prediction. Overflow (underflow) bins are indicated by $>$ ($<$) labels, and are normalized to the width shown.
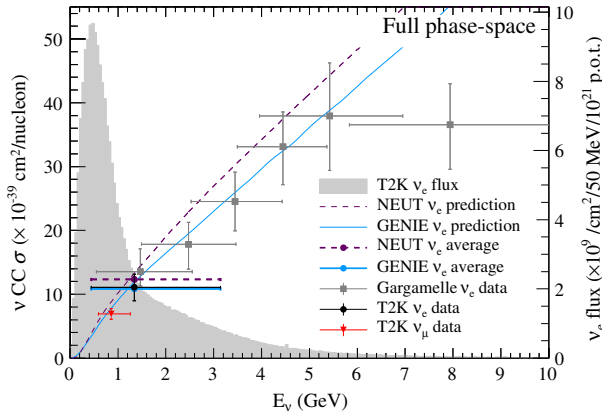
FIG. 3 (color online). Total ν_e CC inclusive cross section when unfolding through Q^2_{QE}. The T2K data point is placed at the ν_e flux mean energy. The vertical error represents the total uncertainty, and the horizontal bar represents 68% of the flux each side of the mean. The T2K flux distribution is shown in gray. The NEUT and GENIE predictions are the total ν_e CC inclusive predictions as a function of neutrino energy. The NEUT and GENIE averages are the flux-averaged predictions. Gargamelle ν_e and T2K ν_μ data are taken from Ref. [9] and Ref. [6], respectively.

agree with both NEUT and GENIE, although a deficit is seen at low Q^2_{QE} compared to NEUT. The biggest differences between NEUT and GENIE at low Q^2_{QE} are caused by the different values of M^{QE}_A chosen for CCQE interactions, and different CC coherent interaction models.

The total flux-averaged cross section when unfolding through Q^2_{QE} is $\langle\sigma\rangle_\phi = 1.11 \pm 0.10(\text{stat}) \pm 0.18(\text{syst})\times$ 10^{-38} cm^2/nucleon, which agrees with both the NEUT prediction of 1.23×10^{-38} cm^2/nucleon and the GENIE prediction of 1.08×10^{-38} cm^2/nucleon. The result is shown in Fig. 3, along with the Gargamelle data from 1978 [9] and T2K ν_μ inclusive cross-section results from Ref. [6]. Both T2K ν_μ and ν_e total flux-averaged cross sections agree well with the predictions but are not directly comparable due to the differences between the ν_μ and ν_e spectra in T2K. The results when unfolding through the other variables agree at the percent level. The dominant systematic uncertainties on this result are the flux (12.9%) and detector systematics (8.4%), with all other systematics giving a 6.1% uncertainty when added in quadrature. The uncertainty from reweighting the out-of-fiducial background is 2.1%.

An important aspect of the Bayesian unfolding approach is that it allows a reconstructed distribution to be unfolded into regions that it is not sensitive to. This analysis has poor reconstruction efficiency for low momentum, backwards going, or high angle electrons. This adds model dependency since the NEUT generator must predict these poorly determined regions. For this reason, a second result is presented in which only events with $p_e > 550$ MeV and $\cos(\theta_e) > 0.72$ are considered. In this "reduced phase-space" result, no attempt is made to unfold into regions of low detector
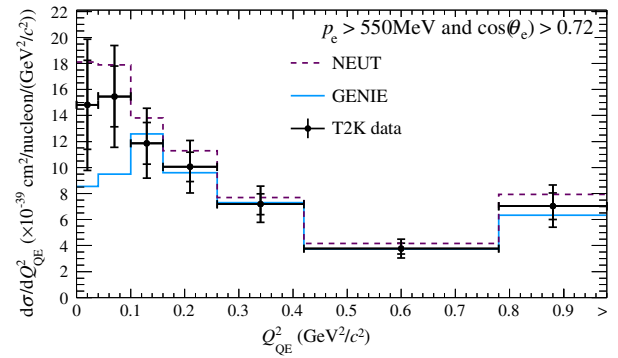

FIG. 4 (color online). Unfolded ν_e CC inclusive differential cross section as a function of Q^2_{QE}, when only electrons with $p_e > 550$ MeV and $\cos(\theta_e) > 0.72$ are considered. The inner (outer) error bars show the statistical (total) uncertainty on the data. The dashed (solid) line shows the NEUT (GENIE) prediction. The overflow bin is indicated by $>$, and is normalized to the width shown.

efficiency. The unfolded Q^2 differential cross-section result for this reduced phase space is shown in Fig. 4.

Conclusion.—Understanding differences between ν_e and ν_μ cross sections is vital as long baseline oscillation experiments search for CP violation in the lepton sector. The T2K off-axis near detector ND280 has been used to extract ν_e CC inclusive flux-averaged differential cross sections as a function of p_e, $\cos(\theta_e)$, and Q^2_{QE}, and they are found to agree with both the NEUT and GENIE neutrino interaction generator predictions. These are the first ever ν_e differential cross-section measurements at the GeV scale. The total ν_e CC inclusive flux-averaged cross section is found to be $1.11 \pm 0.21 \times 10^{-38}$ cm^2/nucleon, which is also in agreement with the NEUT and GENIE predictions. The data related to the measurement can be found in [32].

[*]Deceased.
[†]Also at J-PARC, Tokai, Japan.
[‡]Also at Institute of Particle Physics, Canada.

[§]Affiliated member at Kavli IPMU (WPI), the University of Tokyo, Japan.

[‖]Also at Moscow Institute of Physics and Technology and National Research Nuclear University "MEPhI", Moscow, Russia.

[¶]Also at JINR, Dubna, Russia.

[**]Also at BMCC/CUNY, Science Department, New York, New York, USA.

[1] B. M. Pontecorvo, JETP Lett. **33**, 549 (1957).

[2] Z. Mäki, M. Nakagawa, and S. Sakata, Prog. Theor. Phys. **28**, 870 (1962).

[3] J. Beringer et al. (Particle Data Group), Phys. Rev. D **86**, 010001 (2012).

[4] K. Abe et al. (T2K Collaboration), Phys. Rev. Lett. **112**, 061802 (2014).

[5] J. A. Formaggio and G. P. Zeller, Rev. Mod. Phys. **84**, 1307 (2012).

[6] K. Abe et al. (T2K Collaboration), Phys. Rev. D **87**, 092003 (2013).

[7] B. Tice et al. (MINERvA Collaboration), Phys. Rev. Lett. **112**, 231801 (2014).

[8] G. Fiorentini et al. (MINERvA Collaboration), Phys. Rev. Lett. **111**, 022502 (2013).

[9] J. Blietschau et al. (Gargamelle Collaboration), Nucl. Phys. **B133**, 205 (1978).

[10] M. Day and K. S. McFarland, Phys. Rev. D **86**, 053003 (2012).

[11] K. Abe et al. (T2K Collaboration), Nucl. Instrum. Methods Phys. Res., Sect. A **659**, 106 (2011).

[12] K. Matsuoka et al., Nucl. Instrum. Methods Phys. Res., Sect. A **624**, 591 (2010).

[13] M. Otani et al., Nucl. Instrum. Methods Phys. Res., Sect. A **623**, 368 (2010).

[14] S. Fukuda et al. (Super-Kamiokande Collaboration), Nucl. Instrum. Methods Phys. Res., Sect. A **501**, 418 (2003).

[15] P. Amaudruz et al. (T2K ND280 FGD Collaboration), Nucl. Instrum. Methods Phys. Res., Sect. A **696**, 1 (2012).

[16] N. Abgrall et al. (T2K ND280 TPC Collaboration), Nucl. Instrum. Methods Phys. Res., Sect. A **637**, 25 (2011).

[17] S. Assylbekov et al. (T2K ND280 P0D Collaboration), Nucl. Instrum. Methods Phys. Res., Sect. A **686**, 48 (2012).

[18] D. Allan et al. (T2K UK Collaboration), JINST **8**, P10019 (2013).

[19] S. Aoki et al. (T2K ND280 SMRD Collaboration), Nucl. Instrum. Methods Phys. Res., Sect. A **698**, 135 (2013).

[20] K. Abe et al. (T2K Collaboration), Phys. Rev. D **87**, 012001 (2013).

[21] A. Ferrari, P. Sala, A. Fasso, and J. Ranft, FLUKA: A Multi-Particle Transport Code (2005).

[22] N. Abgrall et al. (NA61/SHINE Collaboration), Phys. Rev. C **84**, 034604 (2011).

[23] N. Abgrall et al. (NA61/SHINE Collaboration), Phys. Rev. C **85**, 035210 (2012).

[24] R. Brun, F. Carminati, and S. Giani, Report No. CERN-W5013, 1994.

[25] C. Zeitnitz and T. A. Gabriel, in Proceedings of the International Conference on Calorimetry in High Energy Physics, 1993.

[26] K. Abe et al. (T2K Collaboration), Nucl. Instrum. Methods Phys. Res., Sect. A **694**, 211 (2012).

[27] K. Abe et al. (T2K Collaboration), Phys. Rev. D **89**, 092003 (2014).

[28] Y. Hayato, Nucl. Phys. B, Proc. Suppl. **112**, 171 (2002).

[29] K. Abe et al. (T2K Collaboration), Phys. Rev. D **88**, 032002 (2013).

[30] G. D'Agostini, Nucl. Instrum. Methods Phys. Res., Sect. A **362**, 487 (1995).

[31] C. Andreopoulos et al., Nucl. Instrum. Methods Phys. Res., Sect. A **614**, 87 (2010).

[32] K. Abe et al., T2K public data, http://t2k-experiment.org/results/nd280-nue-xs-2014.